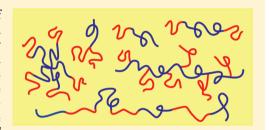# Effect of Architecture on the Phase Behavior of AB-Type Block Copolymer Melts

M. W. Matsen*

School of Mathematical and Physical Sciences, University of Reading, Whiteknights, Reading RG6 6AX, United Kingdom

ABSTRACT: Equilibrium phase diagrams are calculated for a selection of two-component block copolymer architectures using self-consistent field theory (SCFT). The topology of the phase diagrams is relatively unaffected by differences in architecture, but the phase boundaries shift significantly in composition. The shifts are consistent with the decomposition of architectures into constituent units as proposed by Gido and co-workers, but there are significant quantitative deviations from this principle in the intermediate-segregation regime. Although the complex phase windows continue to be dominated by the gyroid (G) phase, the regions of the newly discovered *Fddd* (O^{70}) phase become appreciable for certain architectures and the perforated-lamellar (PL) phase becomes stable when the complex phase windows shift toward high compositional asymmetry.

■ INTRODUCTION

The phase behavior of AB diblock copolymer melts has been well studied experimentally,[1] and self-consistent field theory (SCFT)[2] has been remarkably successful in explaining the equilibrium phase behavior.[3−5] Vavasour and Whitmore[6] produced the first SCFT phase diagram, but it was limited to the classical lamellar (L), cylindrical (C), and bcc spherical (S) phases. Matsen and Schick[7] then extended it to include complex phases, predicting the gyroid (G) phase to be more stable than the perforated-lamellar (PL) phase as confirmed later by experiment.[8] In a subsequent calculation by Matsen and Bates,[9] a narrow closed-packed spherical (S_{cp}) phase was predicted along the order−disorder transition (ODT), which has since been associated with a region of densely packed spherical micelles.[10,11] Most recently, the *Fddd* (O^{70}) phase was predicted by Tyler and Morse[12] and later observed in experiment.[13−15] Figure 1 shows the current up-to-date SCFT phase diagram for AB diblock copolymer melts.

The AB diblock is just the simplest block copolymer among an unlimited variety of different architectures. It is natural to ask how the phase behavior changes for other architectures, but this has proven to be a daunting task as soon as a third chemically distinct component is involved; in fact, even the simple linear ABC triblock exhibits so many morphologies that we might never catalogue them all.[16] Nevertheless, the phase behavior appears manageable for those architectures comprised of just two segment types. Among this class of architectures, the ABA triblock is the next most studied block copolymer,[17] mainly because of its commercial use as a thermoplastic elastomer. There were also a considerable number of early experiments on star block copolymers, formed by joining three or more diblocks together by their ends.[18−20] More recently, though, experiments have focused on miktoarm stars[21−26] and various graft architectures.[27−30] The theoretical work on AB-type architectures is starting to catchup with experiment; SCFT phase diagrams now exist for ABA triblocks,[31,32] linear ABAB...
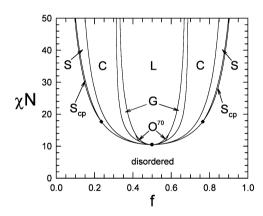

Figure 1. Phase diagram for melts of AB diblock copolymers, showing the stability regions of the ordered lamellar (L), cylindrical (C), bcc spherical (S), hcp spherical (S_{cp}), gyroid (G), and *Fddd* (O^{70}) morphologies. The dot denotes a mean-field critical point, and the diamonds mark a couple of the difficult to resolve triple points.

multiblocks,[33] diblock-arm stars,[34] triblock-arm stars,[35] various miktoarm stars,[35,36] branched diblocks,[37,38] and multigraft combs.[39]

The general conclusion from these studies is that all AB-type architectures have similar phase diagrams, but with significantly shifted phase boundaries. The reason for the similarity is fairly well understood. Although mechanical properties are completely altered by snipping the middle B blocks of an ABA triblock melt in half, the free energy is relatively unaffected, and thus its equilibrium phase diagram remains much the same as that of an AB diblock copolymer melt.[31] The same rational applies to linear ABAB.. multiblocks, and likewise the phase

behavior of diblock-arm stars should be reasonably unaffected by uncoupling their arms. Gido and co-workers[27−29] have taken this idea one step further, decomposing multigraft block copolymers into constituent A_mB_n miktoarm stars and mapping them on to a phase diagram calculated by Milner[40] using the strong-stretching theory (SST) of Semenov,[41] which is the infinite-segregation limit of SCFT.[42] This has been successful in explaining the compositional shift in the phase boundaries.

The effect of architecture on complex phase behavior is less well understood. Experiments are far too time-consuming to thoroughly address this issue, while theoretical calculations have been computationally costly. Consequently, SCFT calculations for the complex phases have been restricted to relatively weak segregations, often with some of the potential phases omitted from consideration. The *Fddd* morphology has never been considered largely because it was not even discovered at the time of most calculations, and similarly many previous studies where not aware of alternatives to the bcc packing of spheres. We now know of other potential arrangements such as close-packed spheres (fcc or hcp) as well as an A15 packing predicted by Grason and Kamien[36] for AB_n miktoarm stars and later confirmed in experiment.[43] Fortunately, there have been a number of recent numerical advances[44−46] that allow the complex phases to be readily examined up to high segregations. Therefore, we now revisit the ABA triblock, linear ABAB... multiblock, diblock-arm star, and AB_2 miktoarm star architectures, updating their phase diagrams from all the known morphologies and mapping the complex phase windows to higher segregation. We also evaluate a new phase diagram for combs with a B-type backbone and A-type teeth, formed by stringing AB_2 stars together, so as to further test if the phase behavior of multigraft block copolymers is equivalent into that of their constituent units.

■ RESULTS

There are ample descriptions of the SCFT for complex architectures in the existing literature,[31−34,38,39] and so we forego any further repetition of the theory. It suffices to say that we perform standard calculations for incompressible melts using the standard Gaussian chain model with conformational symmetry between the A and B segments.[3] Our study considers five different architectures, where the constituent units are either the AB diblock or the AB_2 miktoarm star. The relevant parameters are the number of segments per constituent unit, N, the standard Flory−Huggins interaction parameter, χ, and the volume fraction of the A component, f.

After the AB diblock architecture, the symmetric ABA triblock, formed by joining two identical AB diblocks together by their B ends, is the most common block copolymer. Its phase diagram is shown in Figure 2, which extends the previous calculation[31] to show the gyroid (G) channel to much higher segregation and to include the *Fddd* (O^{70}) morphology. Since the triblock is formed by joining two diblocks together, the phase diagram is expected to be similar to Figure 1 when N is defined as the half of the total polymerization, and indeed it is. Nevertheless, the phase boundaries are shifted somewhat and the symmetry about $f = 0.5$ is now broken. Interestingly, the stability regions of the O^{70} phase are about half again as large as those of the diblock copolymer melt, but the regions of the close-packed spherical (S_{cp}) phase are somewhat narrower.

Naturally, we can create ever larger linear multiblocks by joining more diblocks together by their equivalent ends. As the number of blocks increases, the system reaches an asymptotic
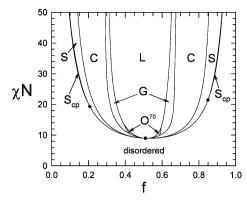

Figure 2. Phase diagram analogous to that of Figure 1, but for symmetric ABA triblock copolymers. Here N is the degree of polymerization of the diblocks formed by snipping the triblocks in half.

limit,[47] previously investigated by Matsen and Schick.[34] Figure 3 extends that calculation by plotting the complex phase
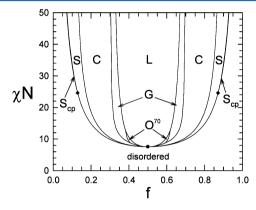

Figure 3. Phase diagram analogous to that of Figure 1, but for infinite linear ABAB... multiblock copolymers. Here N is the degree of polymerization of the diblocks formed by cutting all the blocks in the middle.

channel to far higher segregation and testing for the O^{70}, S_{cp}, and S_{A15} phases. As expected, the topology of the phase diagram remains equivalent to that of the diblock copolymer melt, since the multiblock architecture is just a string of diblocks joined together. In the limit of an infinite number of blocks, the phase diagram again becomes symmetric about $f = 0.5$. Continuing the trend from the diblock to the triblock, the multiblock architecture has slightly larger O^{70} regions and narrower S_{cp} regions.

Another way of joining diblocks together is by connecting, for example, the B-ends to form a diblock-arm star. This is evidently the first system for which experiments[18−20] observed a gyroid morphology, although it was mistakenly identified as a double-diamond morphology. This misassignment was corrected[48] shortly after SCFT calculations[34] predicted gyroid to be more stable than double-diamond. The SCFT calculations, however, only explored the complex phase channel at weak segregations and furthermore did not test for the O^{70}, S_{cp}, and S_{A15} phases. Figure 4 now provides a more complete phase diagram for 9-arm stars. Although the topology of the diagram remains equivalent to that of the diblock, there are particularly large shifts in the phase boundaries. Equally significant is the fact that the O^{70} regions are far bigger than those of the
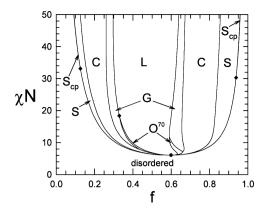
Figure 4. Phase diagram analogous to that of Figure 1, but for 9-arm star block copolymers where each molecule is formed by joining 9 diblocks together by their B-ends. Here N is the degree of polymerization of each diblock arm.

previous architectures, while the S_{cp} regions are particularly narrow.

In general, the constituent units of AB-type architectures are A_mB_n miktoarm stars, where m arms are entirely composed of A segments and n arms are made up of entirely B segments.[27−29] Grason and Kamien[36] have calculated phase diagrams for $m = 1$ with $n = 2, 3, 4,$ and 5, but they did not consider the perforated-lamellar (PL) and $Fddd$ (O^{70}) phases. Therefore, we redo the calculation for the AB_2 star, which is the simplest version beyond the trivial diblock where $m = n = 1$. The new phase diagram in Figure 5 exhibits a sizable O^{70} region on the large-f
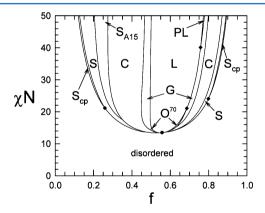

Figure 5. Phase diagram analogous to that of Figure 1, but for AB_2 star block copolymers where each molecule has one A-type arm and two identical B-type arms. The change in architecture results in additional stability regions for the ordered A15 spherical (S_{A15}) and perforated-lamellar (PL) morphologies. Here N is the degree of polymerization of the entire molecule.

side of the diagram, where the B-component forms the network and the A-component forms the matrix. More interestingly, however, is the emergence of a stable PL region on the same side of the phase diagram but at higher segregation. To the best of our knowledge, PL has only been previously predicted to be stable for diblock/homopolymer blends[49,50] and never for a neat block copolymer melt. It is also worth noting that the closed-packed spherical (S_{cp}) regions are substantially larger than for the other architectures.

By joining the AB_2 miktoarm stars together in a series by their B ends, one obtains a comb block copolymer with a B-type backbone and A-type teeth. As our last example, Figure 6
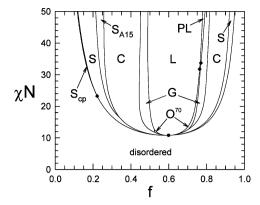
plots the phase diagram of the comb architecture in the limit where it has an infinite number of teeth. The phase diagram for a finite number of teeth will naturally be intermediate to Figures 5 and 6. For the most part, stringing the stars together to form a comb has little effect on the phase diagram, but it does cause a substantial increase in the size of the complex O^{70} and PL regions. There is also a significant narrowing of the S_{cp} regions, so much so that the one on the right vanishes for our range of segregations (i.e., $\chi N \leq 50$).

■ DISCUSSION

According to SST, the free energy of a strongly segregated block copolymer melt should be relatively unaffected by snipping in half those blocks that have both ends constrained to the internal A/B interfaces. This leads to the hypothesis that complex architectures can be decomposed into constituent units,[27−29] implying that Figures 2−4 should closely resemble the AB diblock phase diagram in Figure 1, while Figure 6 should approximately match the AB_2 star block phase diagram in Figure 5. This principle is vaguely accurate near $\chi N \approx 50$ and must become exact in the infinite-segregation limit (i.e., $\chi N \rightarrow \infty$).[42] Nevertheless, there are significant deviations in the intermediate-segregation regime, and there are also considerable shifts in the order−disorder transition (ODT). The latter occurs simply because architectures composed of fewer units result in more free ends per unit volume, and end segments are able to escape their domains more easily than middle segments which promotes the disordered state.

One might suspect that architecture could have a big effect on the complex phase behavior, since the free energy differences between the competing phases are relatively small. However, there is no dramatic change. The gyroid (G) phase continues to dominate the complex phase channel, and the newly discovered $Fddd$ (O^{70}) phase remains stable extending down to the mean-field critical point just as it does for diblock copolymer melts.[51] In the diblock copolymer system, the predicted O^{70} regions are rather small and thus prone to the effect of fluctuations.[52] However, O^{70} does evidently survive fluctuations given the fact that it has been identified by experiments in diblock copolymer melts,[13−15] although this may have been aided by conformational asymmetry.[46] Nevertheless, we can expect the O^{70} phase to be a common feature of AB-type block copolymer melts, given that its predicted stability regions are significantly larger for all the other

Figure 6. Phase diagram analogous to that of Figure 5, but for a comb architecture where the backbone is type B and the regularly spaced teeth are of type A. Here N is the degree of polymerization per tooth.

architectures we examined, particularly so for the star and comb block copolymers.

As expected from the decomposition principle, the A15 spherical (S_{A15}) phase occurs for combs (Figure 6) in the same place that Grason and Kemien[36] predicted it for AB_2 miktoarm stars (Figure 5). Likewise, the perforated-lamellar (PL) phase occurs in the same region of both phase diagrams. Not surprisingly, its occurrence between the L and G morphologies is precisely where it is most metastable in the diblock phase diagram. Even the preferred version of the PL phase, where perforated layers pack in an abcabc... sequence, is the same as in the diblock system.[46] We suspect that PL becomes stable for the star and comb architectures because the complex phase window has been shifted toward high asymmetries, where the majority-component layers are particularly thick. It has been shown that the PL phase is only metastable in diblock copolymers because of packing frustration in its majority-component layers.[53] This conclusion stems from the fact that PL can be stabilized with the addition of majority-component homopolymer.[49,50] Likewise, we attribute the stability of PL in Figures 5 and 6 to a reduction in packing frustration that results from the extra thickness of the majority-component layers.

Just as in the diblock system, all the phase diagrams have triple points (denoted by diamond symbols) along the ODT beyond which there are narrow regions of the close-pack spherical (S_{cp}) phase. Although it is missing from the right side of Figure 6 for the comb architecture, we expect that it does become stable at some point beyond the range of the plot. In all cases, the hcp symmetry was slightly more stable than the fcc packing of spheres as found earlier for the diblock architecture.[46] Although Grason et al.[37,38] predict fcc regions along the ODT for number of different architectures, this is evidently because they did not consider the hcp arrangement. Interestingly, we observe a narrowing of the S_{cp} regions for architectures with more units, which is relatively easy to explain. The S_{cp} phase occurs when the minority-component blocks start pulling out of the spherical domains and swelling the matrix, which relieves the packing frustration responsible for the usual bcc arrangement of spheres. This happens more readily when the minority-component blocks have free ends, and thus the smaller AB diblock and AB_2 star architectures have the larger S_{cp} regions.

Of course, there is still the possibility that a stable morphology is missing from our new phase diagrams. There are screening methods[54,55] that could be used to search for new phases, but it is unclear how effective they are at capturing all the stable phases. So far, the known phases for AB-type block copolymer melts have been found by experimental observation. Even the discovery of the *Fddd* phase in the diblock copolymer system, which was predicted by SCFT[12] two years before it was experimentally identified,[13] is ultimately accredited to experiment. It was only realized as a potential candidate structure after an analogous phase was experimentally identified in ABC triblock copolymer melts.[56] Similarly, the A15 spherical phase was observed in lyotropic liquid crystals,[57] before being considered as a candidate structure for block copolymers.

Our current calculations were made possible by recent numerical developments, whereby the spectral algorithm for evaluating the concentration profiles for given fields was combined with Anderson mixing for solving the self-consistent field equations.[46] We have previously[7,9,31-34] used a quasi-Newton–Raphson algorithm (specifically the Broyden algorithm) to solve the field equations, which requires the calculation of a Jacobian. This works exceptionally well when the morphology requires ≲100 generalized Fourier functions to accurately represent the composition profiles, and thus we still use it in these instances. However, far more Fourier terms are required for triply periodic phases at high segregation, and then the calculation of the Jacobian becomes prohibitive. Fortunately, Anderson mixing is capable of solving the field equations without a Jacobian, which permits calculations involving as many as 5000 basis functions with just a single computer processor. Even though our calculations were performed to high accuracy, we never needed more than 2000 basis functions.

Pseudospectral methods can also be combined with Anderson mixing to produce an efficient algorithm for calculating SCFT phase diagrams.[44] However, the full-spectral method is still generally faster apart from the upper part of the complex phase channel, where the morphologies require ≳1000 basis functions. Furthermore, the spectral method is superior at handling some of the more complex architectures, such as the linear and comb multiblock copolymers in Figures 3 and 6, respectively. The real advantage of the spectral method though is that it only has one source of numerical inaccuracy to contend with, the truncation of the Fourier series. In contrast, the pseudospectral methods have two distinct sources, the finite spatial resolution and the finite step-size along the chain contour, making it far more of a chore to ensure sufficient numerical accuracy.

■ SUMMARY

We have presented complete phase diagrams for six different AB-type block copolymer melts obtained with self-consistent field theory (SCFT). The principle that complex architectures can be decomposed in constituent A_mB_n stars appears to be reasonably accurate at strong segregations, but significant deviations are evident in the intermediate-segregation regime. Nevertheless, the qualitative behavior is preserved. For instance, the ABA triblock, linear ABAB... multiblock and diblock-arm star have phase diagrams that are topologically equivalent to that of the simple AB diblock. In all cases, the gyroid (G) morphology dominates the complex phase channel while the new *Fddd* (O^{70}) microstructure remains stable in small regions extending down to the mean-field critical point. Similarly, the phase diagram for combs with A-type teeth and a B-type backbone has the same topology as that of AB_2 miktoarm stars. In particular, the comb exhibits a stable region of A15 spheres (S_{A15}) in the same place Grason and Kamien[36] predicted it for AB_2 stars, and furthermore both architectures exhibit a perforated-lamellar (PL) morphology with perforations in the B-rich lamellae, which is stable between the L and G phases for well-segregated conditions. The appearance of the PL phase occurs presumably because the complex phase window is shifted toward large *f*, which thickens the A-rich lamellae thereby relieving packing frustration.

The ability to use architecture to control the composition and size of the stability regions in the phase diagram is yet another useful means for designing block copolymer materials. However, investigating the effect of architecture by experiment alone would be extremely time-consuming and costly, and simple principles such as decomposing complex architectures into their constituent units are of limited application and accuracy. Fortunately, recent developments in numerical methods[44-46] allow high-precision SCFT calculations to be performed on even the most complex periodic morphologies

using very modest computational resources. Thus, SCFT will be a particularly valuable tool for navigating the immense variety of possible architectures.

■ AUTHOR INFORMATION

Corresponding Author
*E-mail: m.w.matsen@reading.ac.uk.

Notes
The authors declare no competing financial interest.

■ REFERENCES

(1) Bates, F. S.; Schulz, M. F.; Khandpur, A. K.; Förster, S.; Rosedal, J. H.; Almdal, K.; Mortensen, K. *Faraday Discuss.* **1994**, *98*, 7−18.
(2) Helfand, E. *J. Chem. Phys.* **1975**, *62*, 999−1005.
(3) Matsen, M. W. *J. Phys.: Condens. Matter* **2002**, *14*, R21−R47.
(4) Matsen, M. W. In *Soft Matter: Polymer Melts and Mitures*; Gompper, G., Schick, M., Eds.; Wiley-VCH: Weinheim, Germany, 2006; Vol. *1*, Chapter 2.
(5) Fredrickson, G. H. *The Equilibrium Theory of Inhomogeneous Polymers*; Oxford University Press: New York, 2006.
(6) Vavasour, J. D.; Whitmore, M. D. *Macromolecules* **1992**, *25*, 5477−5486.
(7) Matsen, M. W.; Schick, M. *Phys. Rev. Lett.* **1994**, *27*, 2660−2663.
(8) Hajduk, D. A.; Takenouchi, H.; Hillmyer, M. A.; Bates, F. S.; Vigild, M. E.; Almdal, K. *Macromolecules* **1997**, *30*, 3788−3795.
(9) Matsen, M. W.; Bates, F. S. *Macromolecules* **1996**, *29*, 1091−1098.
(10) Schwab, M.; Stühn, B. *Colloid Polym. Sci.* **1997**, *275*, 341−351.
(11) Han, C. D.; Vaidya, N. Y.; Kim, D.; Shin, G.; Yamaguchi, D.; Hashimoto, T. *Macromolecules* **1998**, *33*, 3767−3780.
(12) Tyler, C. A.; Morse, D. C. *Phys. Rev. Lett.* **2005**, *94*, 208302.
(13) Takenaka, M.; Wakada, T.; Akasaka, S.; Nishitsuji, S.; Saijo, K.; Shimizu, H.; Kim, M. I.; Hasegawa, H. *Macromolecules* **2007**, *40*, 4399−4402.
(14) Kim, M. I.; Wakada, T.; Akasaka, S.; Nishitsuji, S.; Saijo, K.; Hasegawa, H.; Ito, K.; Takenaka, M. *Macromolecules* **2008**, *41*, 7667−7670.
(15) Kim, M. I.; Wakada, T.; Akasaka, S.; Nishitsuji, S.; Saijo, K.; Hasegawa, H.; Ito, K.; Takenaka, M. *Macromolecules* **2009**, *42*, 5266−5271.
(16) Bates, F. S.; Fredrickson, G. H. *Phys. Today* **1999**, *52*, 32−38.
(17) Mai, S.-M.; Mingvanish, W.; Turner, S. C.; Chaiundit, C.; Fairclough, J. P. A.; Heatley, F.; Matsen, M. W.; Ryan, A. J.; Booth, C. *Macromolecules* **2000**, *33*, 5124−5130.
(18) Thomas, E. L.; Alward, D. B.; Kinning, D. J.; Martin, D. C.; Handlin, D. L.; Fetters, L. J. *Macromolecules* **1986**, *19*, 2197−2202.
(19) Alward, D. B.; Kinning, D. J.; Thomas, E. L.; Fetters, L. J. *Macromolecules* **1986**, *19*, 215−224.
(20) Herman, D. S.; Kinning, D. J.; Thomas, E. L.; Fetters, L. J. *Macromolecules* **1987**, *20*, 2940−2942.
(21) Pochan, D. J.; Gido, S. P.; Pispas, S.; Mays, J. W.; Ryan, A. J.; Fairclough, P. A.; Hamley, I. W.; Terrill, N. J. *Macromolecules* **1996**, *29*, 5091−5098.
(22) Pochan, D. J.; Gido, S. P.; Pispas, S.; Mays, J. W. *Macromolecules* **1996**, *29*, 5099−5105.
(23) Gido, S. P.; Lee, C.; Pochan, D. J.; Pispas, S.; Mays, J. W.; Hadjichristidis, N. *Macromolecules* **1996**, *29*, 7022−7028.
(24) Beyer, F. L.; Gido, S. P.; Poulos, Y.; Avgeropoulos, A.; Hadjichristidis, N. *Macromolecules* **1997**, *30*, 2373−2376.
(25) Beyer, F. L.; Gido, S. P.; Uhrig, D.; Mays, J. W.; Bech Tan, N.; Trevino, S. F. *J. Polym. Sci., Part B* **1999**, *37*, 3392−3400.
(26) Yang, L.; Hong, S.; Gido, S. P.; Vellis, G.; Hadjichristidis, N. *Macromolecules* **2001**, *34*, 9069−9073.
(27) Xenidou, M.; Beyer, F. L.; Hadjichristidis, N.; Gido, S. P.; Beck Tan, N. *Macromolecules* **1998**, *31*, 7659−7667.

(28) Lee, C.; Gido, S. P.; Poulos, Y.; Hadjichristidis, N.; Bech Tan, N.; Trevino, S. F.; Mays, J. W. *Polymer* **1998**, *39*, 4631−4638.
(29) Beyer, F.; Gido, S. P.; Buschl, C.; Iatrou, H.; Uhrig, D.; Mays, J. W.; Chang, M.; Garetz, B. A.; Balsara, N.; Bech Tan, N.; Hadjichristidis, N. *Macromolecules* **2000**, *33*, 2039−2048.
(30) Zhu, Y.; Burgaz, E.; Gido, S. P.; Staudinger, U.; Weidisch, R.; Uhrig, D.; Mays, J. W. *Macromolecules* **2006**, *39*, 4428−4436.
(31) Matsen, M. W.; Thompson, R. B. *J. Chem. Phys.* **1999**, *111*, 7139−7146.
(32) Matsen, M. W. *J. Chem. Phys.* **2000**, *113*, 5539−5544.
(33) Matsen, M. W.; Schick, M. *Macromolecules* **1994**, *27*, 7157−7163.
(34) Matsen, M. W.; Schick, M. *Macromolecules* **1994**, *27*, 6761−6767.
(35) Lynd, N. A.; Oyerokun, F. T.; O'Donogue, D. L.; Handlin, D. L. Jr.; Fredrickson, G. H. *Macromolecules* **2010**, *43*, 3479−3486.
(36) Grason, G. M.; Kamien, R. D. *Macromolecules* **2004**, *37*, 7371−7380.
(37) Grason, G. M.; DiDonna, B. A.; Kamien, R. D. *Phys. Rev. Lett.* **2003**, *91*, 058304.
(38) Grason, G. M.; Kamien, R. D. *Phys. Rev. E* **2005**, *71*, 051801.
(39) Wang, L.; Zhang, L.; Lin, J. *J. Chem. Phys.* **2008**, *129*, 114905.
(40) Milner, S. T. *Macromolecules* **1994**, *27*, 2333−2335.
(41) Semenov, A. E. *Sov. Phys. JETP* **1985**, *85*, 733−742.
(42) Matsen, M. W. *Eur. Phys. J. E* **2010**, *33*, 297−306.
(43) Cho, B.-K.; Jain, A.; Gruner, S. M.; Wiesner, U. *Science* **2004**, *305*, 1598−1601.
(44) Stasiak, P.; Matsen, M. W. *Eur. Phys. J. E* **2011**, *34*, 110.
(45) Cochran, E. W.; Garcia-Cervera, C. J.; Fredrickson, G. H. *Macromolecules* **2006**, *39*, 2449−2451.
(46) Matsen, M. W. *Eur. Phys. J. E* **2009**, *30*, 361−369.
(47) Kavassalis, T. A.; Whitmore, M. D. *Macromolecules* **1991**, *24*, 5340−5345.
(48) Hajduk, D. A.; Harper, P. E.; Gruner, S. M.; Honeker, C. C.; Thomas, E. L.; Fetters, L. J. *Macromolecules* **1995**, *28*, 2570−2573.
(49) Matsen, M. W. *Phys. Rev. Lett.* **1995**, *74*, 4225−4228.
(50) Matsen, M. W. *Macromolecules* **1995**, *27*, 5765−5773.
(51) Ranjan, A.; Morse, D. C. *Phys. Rev. E* **2006**, *74*, 011803.
(52) Miao, B.; Wickham, R. A. *J. Chem. Phys.* **2008**, *128*, 054902.
(53) Matsen, M. W.; Bates, F. S. *Macromolecules* **1996**, *29*, 7641−7644.
(54) Drolet, F.; Fredrickson, G. H. *Phys. Rev. Lett.* **1999**, *83*, 4317−4320.
(55) Guo, Z. J.; Zhang, G. J.; Qiu, F.; Zhang, H. D.; Yang, Y. L.; Shi, A.-C. *Phys. Rev. Lett.* **2008**, *101*, 028301.
(56) Bailey, T. S.; Hardy, C. M.; Epps, T. H.; Bates, F. S. *Macromolecules* **2002**, *35*, 7007−7017.
(57) Sakya, P.; Seddon, J. M.; Templer, R. H.; Mirkin, R. J.; Tiddy, G. J. T. *Langmuir* **1997**, *13*, 3706−3714.